Interaction Strength of Steel-Concrete Composite Beam-Columns Including the Balance Point

Mark D. Denavit

Note: A version of this paper appears in the proceedings of the 2020 Structural Stability Research Council (SSRC) Annual Stability Conference

ABSTRACT

The maximum bending moment capacity of steel-concrete composite column cross sections occurs with concurrently applied axial compression. This is seen in the shape of the interaction diagram, where the bending moment capacity increases with increasing axial compression before reaching the balance point. The size of this bulged region of the interaction diagram can be significant, especially for concrete-dominant sections. However, it is often neglected in design because of two stability-related concerns. First, the simple transformations that are recommended to convert cross-section strength to member strength produce illogical results near the balance point, with member strength exceeding cross-section strength. Second, research has shown that the stiffness reductions used in elastic analyses are not sufficient for highly slender concrete-dominant composite members subjected to high bending moments. This work seeks to address these issues through the development of more advanced transformations and stiffness reductions. These new recommendations will more accurately capture the strength of composite members and allow for more efficient designs.

Keywords: composite construction, interaction strength, balance point, stiffness reduction.

INTRODUCTION

Steel-concrete composite frames are an effective alternative to structural steel or reinforced concrete frames for use as the primary lateral-force-resisting system of building structures. However, they have not yet been as widely adopted in United States practice as they have in other parts of the world, notably East Asia. There are several barriers to the broader use of composite structures. Sequencing issues in construction, which can lead to complications such as difficult coordination of trades, can be a barrier. On the other hand, innovative composite construction methods that resolve the sequencing issues can be highly efficient and can reduce construction time (Griffis, 1992; Traut-Todaro, 2019). Current design provisions are another barrier to the wider adoption of composite construction. Despite recent advances (e.g., Lai et al., 2015; Denavit et al., 2016; Bruneau et al., 2018), design provisions for composite frames are not yet as comprehensive as those for the more traditional systems, nor do they consistently reflect the advantages of composite framing.

Composite columns were introduced to the AISC *Specification for Structural Steel Buildings*, hereafter referred to as the AISC *Specification*, in the 1986 edition (AISC, 1986). From that time until major revisions were made in the 2005 edition (AISC, 2005), the axial and flexural strengths of composite beam-columns were based on calculations that determined an equivalent steel section. This approach had limitations in that it was not applicable to columns with steel ratios below 4%, and it often underestimated the contribution of the concrete, particularly for concrete-dominant composite beam-columns with low steel ratios (Griffis, 2005). The current beam-column strength interaction provisions (AISC, 2016) are based more directly on mechanics principles. The cross-section strength may now be determined using one of several methods; the two most commonly used are the plastic stress distribution method, which is applicable to most common composite column cross sections, and the more general strain-compatibility method, which is comparable to approaches often taken to compute reinforced concrete section strength. The plastic stress distribution method is the primary method for assessing steel-concrete composite columns in the AISC *Specification* (AISC, 2016) and other standards worldwide (CEN, 2004; SAC, 2014). It is accurate over a wide range of materials, cross-sectional geometries, and loading conditions, but the method does result in significant unconservative error for some cases. Cases of unconservative error include encased composite members, also known as steel-reinforced concrete (SRC) members, with high steel ratio, high steel yield stress, or both (Behnam and Denavit, 2020). The strain-compatibility method is conservative in nearly all cases but can be overly conservative in many cases. The

Mark D. Denavit, Assistant Professor, The University of Tennessee, Knoxville, Knoxville, Tenn. Email: mdenavit@utk.edu

Paper No. 2020-11

revisions in the 2005 edition also included an expansion of the range of applicability of the provisions to members with steel ratios as low as 1%.

Using the plastic stress distribution method, pairs of axial compression and bending moment strength are computed based on assumed plastic neutral axis locations. Selecting many possible locations for the plastic neutral axis results in an essentially continuous curve for the interaction diagram. For example, the interaction diagram for the SRC cross section shown in Figure 1 for bending about the major axis of the steel shape is shown in Figure 2(a). This cross section has outside dimensions of 28 in. × 28 in., a W10×49 wide-flange steel shape, and four #8 reinforcing steel bars. The steel ratio (i.e., the ratio of area of steel to gross area of the cross section) for this cross section is $\rho_s = A_s/A_g$ = 1.81% (note that, for simplicity, the fillets between the web and the flange are neglected in this work). The reinforcing ratio (i.e., the ratio of area of reinforcing steel to gross area of the cross section) for this cross section is $\rho_{sr} = A_{sr}/A_g$ = 0.40%. The concrete compressive strength is f'_c = 8 ksi, the steel yield stress is F_y = 50 ksi, and reinforcing steel yield strength is F_{yr} = 60 ksi. The longitudinal reinforcing has a cover of 1⅞ in. from the edge of the concrete to the edge of the bar.

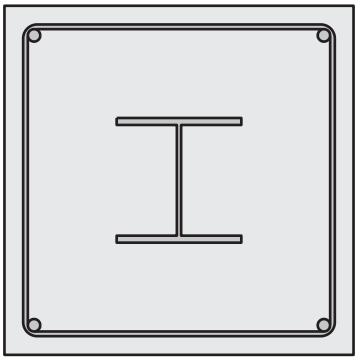

Fig. 1. Example SRC cross section.

The example cross section shown in Figure 1 was selected to have low steel ratios, near the lower limits given in the AISC *Specification* (AISC, 2016) since neglecting the balance point reduces the available strength for concrete-dominant members more than it does for steel-dominant members. This cross section is used in example analyses described throughout this paper.

While the plastic stress distribution method can be used to compute a continuous cross-section interaction diagram by selecting many different plastic neutral axis locations, doing so is burdensome by hand or spreadsheet. A set of closed-form equations (AISC, 2017) has been developed to compute key points on the curve which can then be used to construct a multilinear interaction diagram. The points are labeled A, C, D, and B as shown in Figure 2(a). Point A represents the pure axial strength; point B represents the pure bending strength; point C has the same bending moment as point B, but with axial compression; point D represents the balance point, the point of maximum bending moment.

Computing the cross-section interaction strength is relatively straightforward; however, it is not directly used in

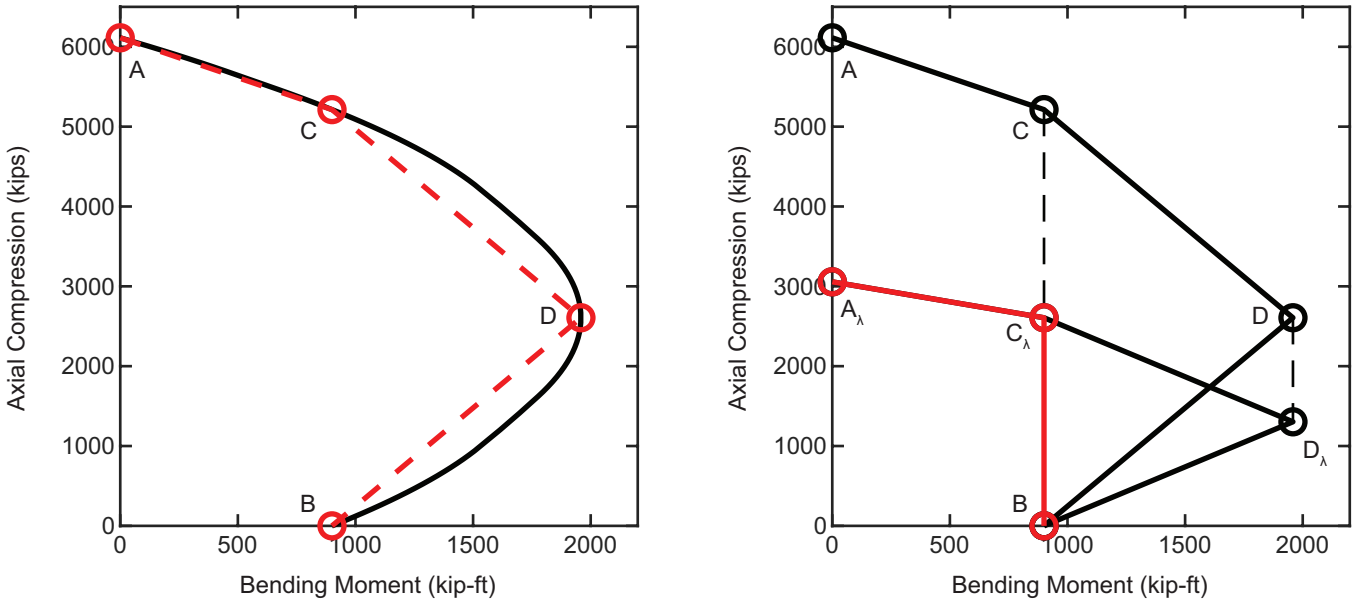

(a) Continuous vs. discrete (ACDB)

(b) Cross-section strength vs. beam-column strength

Fig. 2. Interaction strength diagrams for the example SRC cross section.

design. As described in the AISC *Specification* Commentary (AISC, 2016), two reductions are applied to the nominal cross-section interaction strength to obtain the available beam-column interaction strength.

The first is a stability reduction, where a factor equal to the ratio of the nominal axial compression strength with and without length effects ($\chi = P_n/P_{no}$) is applied to the ordinate (i.e., axial compression) of each point on the interaction diagram, leaving the abscissa (i.e., bending moment) unchanged. This method is logical in that it yields the proper results for pure axial compression (point A) and for pure bending moment (point B), but illogical and potentially unconservative results arise in the intermediate points, particularly the balance point (point D). The balance point is the point of maximum moment and it occurs for a nonzero axial compression. When the stability reduction is applied in this simple manner, the resulting beam-column interaction point D lies outside of the cross-section interaction diagram, as shown in Figure 2(b). Note that the beam-column strength interaction diagram shown in Figure 2(b) was constructed with $\chi = 0.5$, which corresponds to $L_c/H = 18.6$ for the example cross section.

The second reduction is to apply the resistance factors. The resistance factors for composite columns are defined as $\phi_c = 0.75$ for axial compression and $\phi_b = 0.90$ for flexure in AISC *Specification* Chapter I (AISC, 2016). For combined bending and axial load, the AISC *Specification* Commentary recommends that axial compression of each point be multiplied by ϕ_c and the bending moment of each point be multiplied by ϕ_b. This simple procedure may be unconservative because it can lead to strength reductions which imply resistance factors greater than 0.90 for the intermediate points (Denavit, 2017).

Furthermore, when evaluated against advanced second-order inelastic analyses, current design provisions can result in unconservative errors for highly slender, concrete-dominant composite members subject to low axial loads and high bending moments (Denavit et al., 2016). Concerns resulting from the simple reductions and potential unconservative error have led to the recommendation in the AISC *Specification* Commentary to neglect point D in the strength interaction diagram and to only consider points A, C, and B (AISC, 2016).

Neglecting the balance point can be highly conservative, especially for stocky concrete-dominant columns. Improved methods of determining interaction strength of steel-concrete composite beam-columns would have the potential of unlocking large amounts of strength and allowing composite columns to fulfil more of their potential. This work explores potential alternative approaches for including the balance point within the interaction strength of steel-concrete composite beam-columns. This work has two complimentary goals. The first goal is to reduce conservative error introduced by neglecting the balance point. The second goal is to reduce the unconservative error observed for highly slender, concrete-dominant composite members, which may be exacerbated by the inclusion of the balance point. To accomplish these goals, an alternative stability reduction for interaction diagrams and an alternative stiffness reduction to be used with the direct analysis method are evaluated.

ALTERNATIVE STABILITY REDUCTION FOR INTERACTION DIAGRAMS

As described in the previous section, the method for computing the interaction strength of steel-concrete composite columns, which is referred to as Simplified Method 2 in the AISC *Specification* Commentary (AISC, 2016), neglects the balance point (point D). While any number of points on the cross-section interaction diagram can be computed, only three points, A, C, and B are utilized for the available strength of composite beam-columns. Interaction diagrams computed following these recommendations for the example SRC cross section and for a variety of effective lengths are shown in Figure 3(a). The conservativeness of neglecting point D can be seen by comparing the interaction diagrams in Figure 3(a) to the cross-section interaction diagram shown in Figure 2(a). The example SRC cross section is concrete-dominant, so the moment strength at point D is significantly greater than that at point B.

Interaction diagrams using an alternative method of applying the stability reduction are shown in Figure 3(b). In this alternative method, points A, C, and B are computed and reduced as before (i.e., factoring the ordinate by $\chi = P_n/P_{no}$). Noting that factoring just the ordinate for point D gives the illogical result of a point on the beam-column interaction strength diagram outside of the cross-section interaction strength diagram, both the ordinate and the abscissa of point D are reduced. The ordinate of point D is reduced by the same factor as the other points. The abscissa is reduced such that the reduced point D remains on the line between point B and the original point D, thus ensuring that the beam-column interaction strength does not exceed the cross-section interaction strength. A summary of the reduction applied to each point is presented in Table 1.

The interaction diagram including point D and constructed using the alternative stability reduction (denoted as the ACDB interaction) provides a plausible alternative to the interaction diagram currently recommended in the AISC *Specification* Commentary (AISC, 2016) (denoted as the ACB interaction). However, the new interaction diagram must be rigorously evaluated to ensure that it results in safe designs.

When evaluating design provisions for beam-column interaction strength, simply comparing available strengths

Table 1. Points on the Interaction Diagram				
	Cross-Section Strength		Beam-Column Strength	
Point	***M***	***P***	***M***	***P***
A	0	P_A	0	χP_A
C	M_C	P_C	M_C	χP_C
D[a]	M_D	P_D	$(1-\chi)M_B + \chi M_D$	χP_D
B	M_B	0	M_B	0

[a] Point D is not included with the ACB interaction diagram.

computed per design equations to the results of physical experiments or advanced inelastic analyses can be misleading. In practice, available strengths are evaluated against required strengths and required strengths are computed following particular rules (e.g., specific type of analysis, defined stiffness). The provisions for an entire method of design, encompassing both the available and required strengths, must be considered in the evaluation.

Many notable studies have been conducted in this way, including for structural steel columns and the development of the interaction equations in use today (Kanchanalai, 1977), for reinforced concrete columns (Hage and MacGregor, 1974), for the development of the direct analysis method (Surovek-Maleck and White, 2004), and for the extension of the direct analysis method to composite frames (Denavit et al., 2016). Each of these studies duly considered both the calculation of available strength and required strength in their evaluations, albeit using somewhat different approaches. This work expands upon the results presented by Denavit et al. (2016). The approach taken is to compare, for many different individual cases, the maximum applied loads permitted by the design methodology to the applied loads at which failure occurs according to second-order inelastic analyses.

Benchmark Frames

The cases investigated are small frames that consist of a single composite column as shown in Figure 4. The same broad range of cross-section and frame parameters investigated by Denavit et al. (2016) were used in this work.

Four categories of cross section were investigated: (1) circular concrete-filled steel tubes (CCFT), (2) rectangular concrete-filled steel tubes (RCFT), (3) SRC subjected to major-axis bending, and (4) SRC subjected to minor-axis bending. Within these groups, sections were selected to

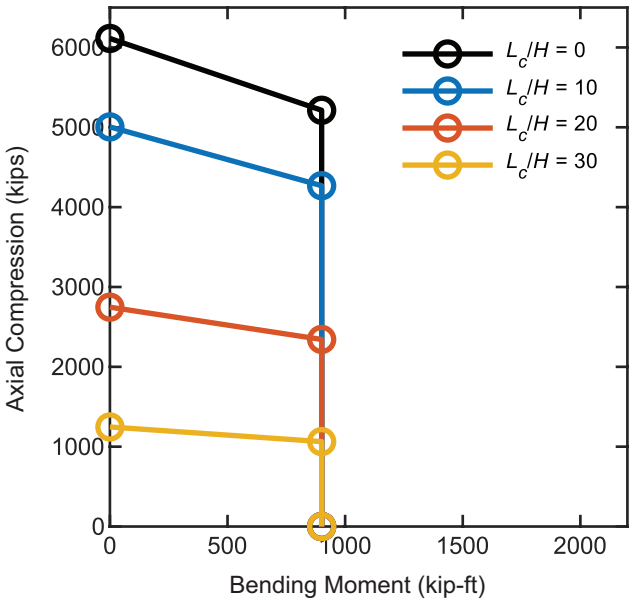

(a) Simplified method 2 (ACB)

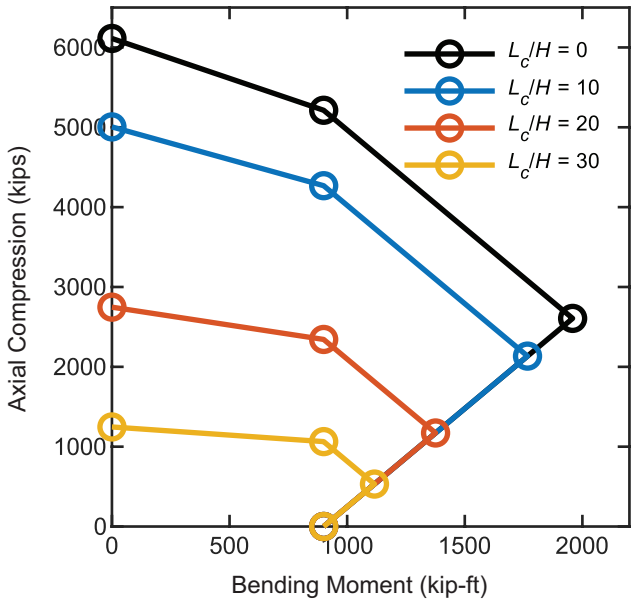

(b) Proposed method (ACDB)

Fig. 3. Interaction strength diagrams for beam-columns with the example SRC cross section.

span practical ranges of concrete strength; steel ratio; and, for the SRC sections, reinforcing ratio. Steel yield strengths were selected as F_y = 50 ksi for wide-flange shapes, F_y = 42 ksi for round HSS shapes, F_y = 46 ksi for rectangular HSS shapes, and F_{ysr} = 60 ksi for reinforcing bars. Three concrete strengths were selected: f'_c = 4, 8, and 16 ksi. Note that the AISC *Specification* (AISC, 2016) limits concrete strength to a maximum of 10 ksi. Concrete exceeding this limit was included to investigate an extreme case and because the limits may be revised in future editions.

With the selected CFT sections, the full range of permitted steel ratios is examined, including those associated with noncompact and slender sections. However, local buckling is neglected in this study, both by not modeling it in the inelastic analyses and by not including the strength reductions in the design strength calculations. The effects of local buckling on the interaction strength of filled composite members can be captured in design through the use of the effective stress-strain method defined in AISC *Specification* Section I1.2 (AISC, 2016) and in analysis through the use of beam elements with specialized constitutive relations or shell elements (Lai and Varma, 2016). Nonetheless, local buckling remains a complicated issue that was excluded from this work for simplicity. Thus, the results of this study are only strictly applicable to compact sections.

As shown in Figure 4, both sidesway inhibited and sidesway uninhibited cases were investigated. The frames are based on and expanded from those used in previous studies (Kanchanalai, 1977; Surovek-Maleck and White, 2004). For the sidesway inhibited frames, a range of column lengths, L, and end moment ratios, β, were investigated. For the sidesway uninhibited frames, a range of column lengths, L, leaning column load ratios, γ, and end restraints (rotational spring stiffnesses, $k_{\theta,top}$ and $k_{\theta,bot}$) were investigated. Each cross section was run with each frame resulting in 1,200 individual cases for each of the CCFT and RCFT groups and 2,880 individual cases for each of the SRC groups. Full details of the selected benchmark frames are reported by Denavit et al. (2016).

Second-Order Inelastic Analysis

Geometric and material nonlinear analyses using fiber-based beam finite elements were used to obtain results against which the design methodologies are benchmarked. These analyses represent the "best guess" of the true behavior of the frames. The uniaxial constitutive relations defined within the fiber representations of the cross sections were calibrated specifically for composite columns. As noted previously, local buckling of the steel tube and other steel components was neglected. Initial system and member geometric imperfections were directly modeled. Full details of the analyses, including validation against the results of hundreds of physical experiments are reported by Denavit et al. (2016) and Denavit and Hajjar (2014).

A sample of analysis results is presented in Figure 5 for various lengths of the sidesway inhibited frame with β = 1 and with the example SRC cross section shown in Figure 1 and described previously. A series of analyses was performed to obtain the results for each individual case shown in Figure 5. First, an analysis applying only vertical load (i.e., M = 0; see Figure 4) was performed to determine the peak load. In this analysis, load was applied and increased in displacement control until a limit point was determined. The limit point was defined as when the lowest eigenvalue

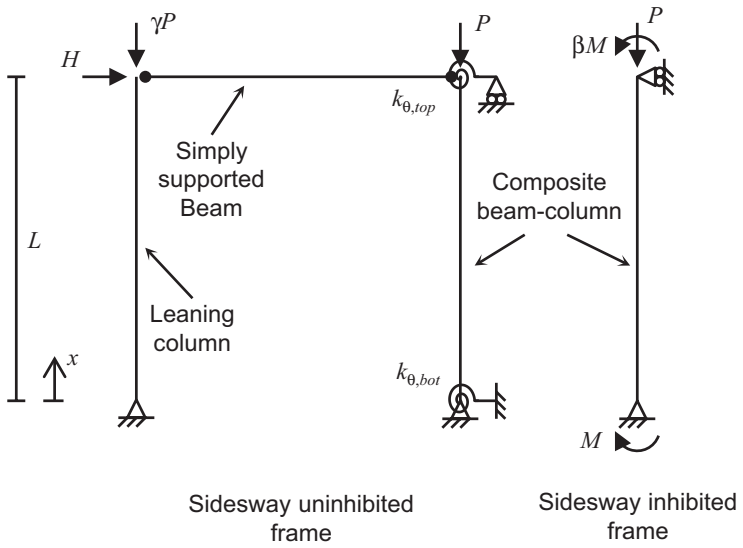

Fig. 4. Benchmark frames.

of the stiffness matrix was equal to zero. This coincides with the maximum applied axial compression. Then, eight separate nonproportional analyses were performed with different values of axial compression equally spaced from zero to the maximum applied axial compression from the axial-only analysis. In each of these nonproportional analyses, the specified level of axial compression is applied in load control then held constant. Subsequently, the lateral load is applied and increased in displacement control until a limit point was determined. The limit point was defined as when the lowest eigenvalue of the stiffness matrix was equal to zero. This coincides with the maximum applied moment. In each analysis, the applied loads and maximum internal forces at the limit point are recorded. These are the values shown in Figure 5. The same process was used for all other interaction diagrams developed using second-order inelastic analyses in this work.

Design Methodology

The maximum applied loads permitted by the design methodology are obtained from an automated iterative process as the applied loads that produce maximum internal forces from an elastic analysis that lay directly on the design interaction diagram [either the ACB such as shown in Figure 3(a) or the ACDB interaction such as shown in Figure 3(b)]. The elastic analyses are performed by evaluating closed-form solutions to the governing differential equation for the benchmark frames obtained from a computer algebra system. Only flexural deformations are considered. The nominal flexural stiffness of the composite columns is taken as EI_{eff} as defined in the AISC *Specification* (AISC, 2016). All stiffnesses are reduced by 0.8, and the flexural stiffness of the composite column is reduced by an additional factor $\tau_b = 0.8$. A notional lateral load of 0.002 times the vertical load was included. The notional load was taken as an additive load when the ratio of second-order drift to first-order drift was greater than or equal to 1.7. It was taken as a minimum lateral load otherwise. A sample of results is presented in Figure 6(a) for the example SRC cross section and the same frames investigated in Figure 5.

Results

The key result from these analyses is the error measured along a radial line from the origin between the interaction diagrams constructed from the maximum applied loads permitted by the design methodology and the applied loads at which failure occurs according to the second-order inelastic analyses. A sample comparison is shown in Figure 6(b) for the example SRC cross section and the sidesway inhibited frame with $L/H = 40$, where H is the lateral dimension of the cross section. For higher axial loads the interaction diagram constructed from the inelastic analyses is outside the interaction diagram constructed from the design methodology, indicating conservative error of up to 70%. For higher bending moments the opposite is true, albeit to a lesser degree, with maximum unconservative error of up to 8%. In this range, the design methodology permits applied loads that the inelastic analysis indicates would result in failure.

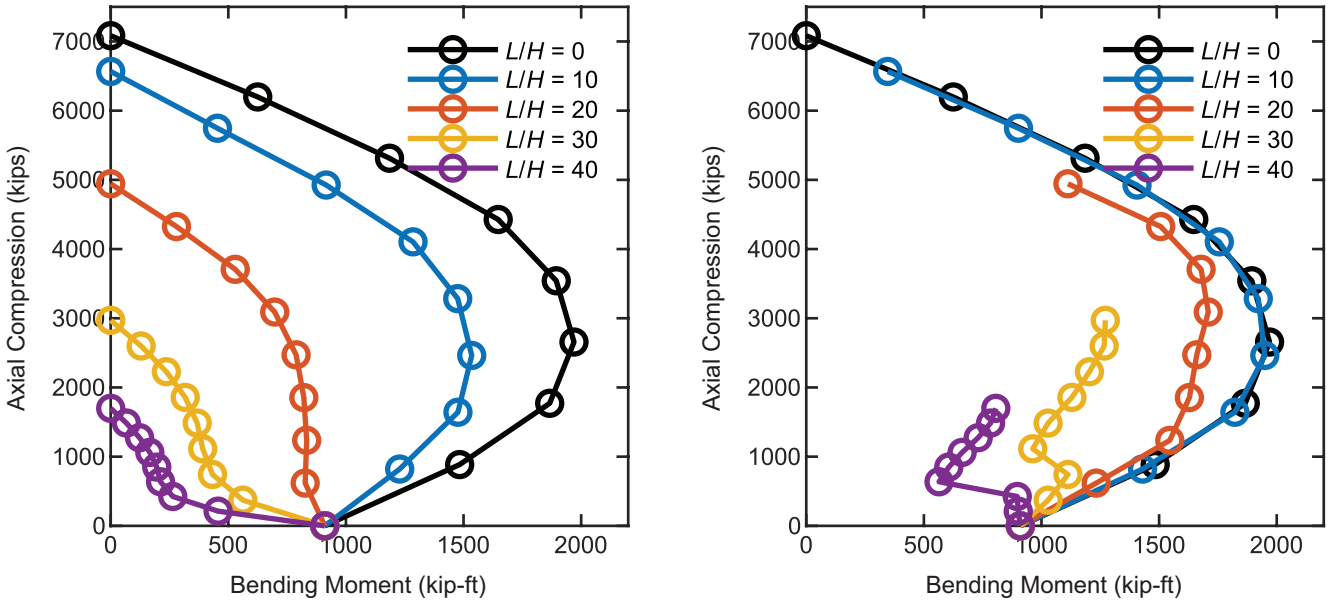

(a) Applied loads *(b) Internal forces*

Fig. 5. Second-order inelastic analysis results for frames with the example SRC cross section.

The error was evaluated for all benchmark frames, at many angles within the *M-P* plane, and for both the ACB and ACDB interaction diagrams. While the selected cross sections and frame parameters can be considered to span the practical range, the distribution of parameters within the selection may not be representative of what is expected in practice. For instance, the selected set contains a far higher proportion of very slender frames than would be expected in typical construction. Accordingly, maximum and minimum error values are more meaningful than median or average error values. Two of the most influential parameters within the set are the steel ratio, ρ_s, and the slenderness. Slenderness is defined by the parameter λ_{oe} (Equation 1) which is proportional to the effective length of the columns. An effective length factor was computed and used for determining λ_{oe} (note, however, that the available strength was computed with an effective length factor of unity in accordance with the direct analysis method). The frames were separated into bins based on ranges of steel ratio and slenderness to better understand the error. The ranges used to separate the frames based on slenderness are shown in Table 2. The maximum unconservative error for each of the bins for the ACDB interaction is shown in Table 3.

$$\lambda_{oe} = \sqrt{\frac{P_{no}}{P_e}} \tag{1}$$

$$P_e = \frac{\pi^2 EI_{eff}}{(KL)^2} \tag{2}$$

The maximum unconservative error varies significantly with section type, slenderness, and steel ratio. The greatest unconservative errors are seen for the slenderest and most concrete-dominant cases. There is no specified limit on the level of unconservative error that can be tolerated within a design methodology. One reference identifies a 5% unconservative error as a reasonable maximum (ASCE, 1997). Another study identified unconservative errors as large as 16% for structural steel columns designed according to the direct analysis method with direct modeling of member imperfections (Wang and Ziemian, 2019). It is important to note that large unconservative errors have been found using the ACB interaction as well (Denavit et al., 2016). Given that the ACDB interaction diagram is larger than the ACB interaction diagram, use of the ACDB interaction diagram can only increase the maximum unconservative errors. The increase in maximum unconservative error for each bin is presented in Table 4. Compared to the magnitude of error, the increase due to the inclusion of point D is modest.

The primary reason to include point D is to reduce conservative error in the evaluation of strength. The decrease in maximum conservative error by including point D for each bin is presented in Table 5. As expected, the largest decreases in conservative error occur for stockier and more concrete-dominant frames. This range is likely more practical and common in construction than the highly slender members for which the high unconservative errors are seen, indicating that the addition of point D would be highly beneficial. Nonetheless, given the increases in

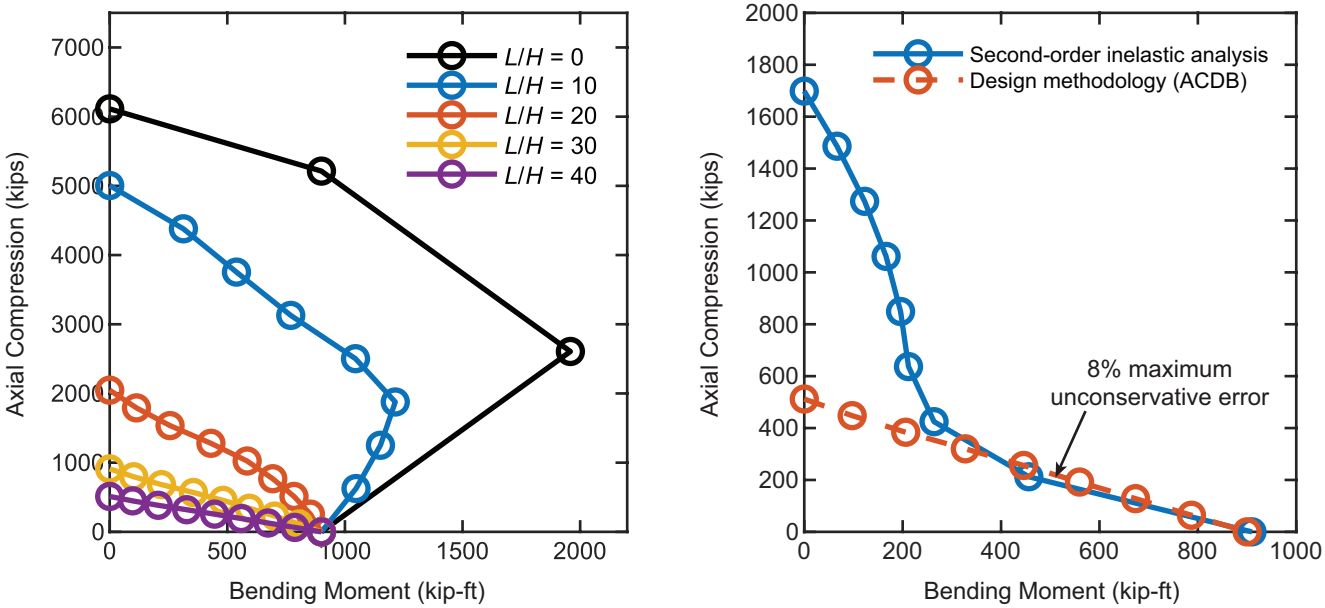

(a) Design methodology—ACDB interaction *(b) Comparison with OpenSees (L/H = 40)*

Fig. 6. Maximum permitted applied loads for frames with the example SRC cross section.

Table 2. Definition of Slenderness Ranges	
Range	**Slenderness**
I	$\lambda_{oe} \leq 0.5$
II	$0.5 < \lambda_{oe} \leq 1.0$
III	$1.0 < \lambda_{oe} \leq 1.5$
IV	$1.5 < \lambda_{oe} \leq 2.0$
V	$2.0 < \lambda_{oe} \leq 3.0$
VI	$3.0 < \lambda_{oe}$

Table 3. Maximum Unconservative Error Based on Slenderness and Steel Ratio, ACDB Interaction							
	ρ_s	I	II	III	IV	V	VI
CCFT	0.25	6.00%	14.6%	12.5%	13.7%	5.70%	5.90%
	0.18	4.40%	12.4%	14.0%	15.9%	8.60%	9.10%
	0.11	5.20%	9.50%	14.4%	17.9%	11.4%	12.8%
	0.06	6.40%	8.90%	11.7%	12.7%	19.3%	17.9%
	0.02	5.40%	6.70%	7.00%	15.6%	24.8%	36.3%
RCFT	0.28	1.70%	2.40%	1.90%	3.00%	0.00%	0.00%
	0.19	4.30%	3.60%	5.20%	7.00%	0.90%	1.30%
	0.11	4.00%	4.60%	8.20%	11.4%	6.30%	7.10%
	0.06	3.90%	4.90%	8.70%	6.20%	16.3%	15.7%
	0.03	1.60%	0.50%	4.80%	10.5%	18.7%	21.8%
SRC major-axis	0.12	6.90%	5.90%	3.60%	4.70%	6.80%	2.10%
	0.09	4.70%	3.60%	3.80%	6.70%	8.90%	4.00%
	0.04	2.00%	0.90%	2.40%	9.70%	14.3%	13.1%
	0.01	2.10%	2.10%	5.00%	7.40%	14.7%	29.2%
SRC minor-axis	0.12	17.4%	15.8%	14.9%	13.9%	14.1%	8.60%
	0.09	13.8%	14.6%	10.3%	12.8%	13.0%	6.80%
	0.04	5.50%	5.70%	8.00%	11.0%	13.8%	11.4%
	0.01	2.10%	2.10%	4.30%	7.50%	11.2%	28.1%

maximum unconservative error, this approach cannot be recommended for general use unless paired with additional changes that reduce the maximum unconservative errors.

ALTERNATIVE STIFFNESS REDUCTION

The previous section addressed the source of some of the greatest conservative errors that exist in the provisions for steel-concrete composite columns. The ACDB interaction diagram significantly reduced the level of conservative error while only modestly increasing the unconservative error. However, the unconservative error was already high in some cases. The greatest unconservative errors occur for highly slender, concrete-dominant members with large flexural demands. Cases such as these are perhaps not often seen in practice, since most engineers wisely avoid this range. However, there is no slenderness limit within the AISC *Specification* (AISC, 2016) and thus cases for which large errors are recorded are permitted. One remedy to these high errors would be to further reduce the size of the interaction diagram. However, a different remedy related to the stiffness reduction may be more appropriate.

The errors occur with low axial loads and high bending moments. High levels of concrete cracking are expected in composite columns under this loading, which is more beam-like than column-like. The flexural rigidity used for composite columns when determining required strengths within the direct analysis method is $0.8\tau_b EI_{eff}$, where

Table 4. Percentage Point Increase in Maximum Unconservative Error Based on Slenderness and Steel Ratio							
	ρ_s	I	II	III	IV	V	VI
CCFT	0.25	3.00%	0.00%	2.50%	1.50%	1.00%	0.70%
	0.18	2.00%	0.00%	3.90%	2.20%	1.30%	1.00%
	0.11	2.40%	2.70%	5.10%	4.00%	3.10%	1.70%
	0.06	0.40%	3.20%	3.20%	6.40%	6.30%	3.10%
	0.02	0.00%	0.40%	7.00%	9.20%	7.70%	7.50%
RCFT	0.28	0.00%	0.00%	1.90%	1.20%	0.00%	0.00%
	0.19	0.00%	0.00%	2.40%	1.90%	0.90%	0.90%
	0.11	0.00%	1.70%	4.00%	3.70%	2.20%	1.70%
	0.06	0.10%	2.60%	4.50%	5.50%	7.10%	3.50%
	0.03	0.00%	0.00%	4.80%	6.20%	7.70%	4.80%
SRC major-axis	0.12	0.00%	0.00%	2.20%	2.30%	2.40%	0.70%
	0.09	0.20%	0.30%	2.30%	4.80%	2.60%	1.20%
	0.04	1.00%	0.20%	1.70%	6.20%	4.70%	2.00%
	0.01	0.00%	0.00%	2.90%	3.30%	3.00%	4.80%
SRC minor-axis	0.12	0.00%	0.50%	0.20%	0.40%	0.20%	0.10%
	0.09	0.30%	0.30%	0.70%	0.40%	0.20%	0.50%
	0.04	0.00%	1.90%	1.80%	0.80%	2.70%	1.40%
	0.01	0.00%	0.00%	2.20%	3.10%	3.40%	4.50%

Table 5. Percentage Point Decrease in Maximum Conservative Error Based on Slenderness and Steel Ratio							
	ρ_s	I	II	III	IV	V	VI
CCFT	0.25	0.00%	0.00%	0.00%	0.00%	0.00%	0.00%
	0.18	0.00%	5.40%	0.00%	0.30%	0.00%	0.00%
	0.11	14.4%	16.5%	1.40%	0.60%	0.80%	0.10%
	0.06	32.4%	28.8%	11.7%	3.20%	1.10%	0.70%
	0.02	33.6%	32.3%	25.5%	9.20%	4.50%	2.10%
RCFT	0.28	0.00%	0.00%	0.00%	0.00%	0.00%	0.00%
	0.19	5.20%	0.00%	0.20%	0.40%	0.00%	0.00%
	0.11	16.9%	10.6%	1.80%	0.70%	0.80%	0.00%
	0.06	31.9%	21.1%	4.70%	2.70%	0.00%	0.70%
	0.03	34.4%	33.4%	18.2%	4.40%	1.60%	1.20%
SRC major-axis	0.12	13.7%	0.00%	0.80%	0.50%	0.30%	0.30%
	0.09	20.6%	6.20%	1.00%	0.80%	0.30%	0.30%
	0.04	30.7%	12.6%	2.20%	0.70%	1.10%	0.30%
	0.01	30.3%	29.0%	10.6%	2.40%	2.20%	0.00%
SRC minor-axis	0.12	0.00%	0.00%	0.30%	0.40%	0.00%	0.20%
	0.09	5.90%	4.10%	1.10%	0.50%	0.00%	0.10%
	0.04	28.2%	9.50%	0.90%	0.40%	0.70%	0.20%
	0.01	30.2%	28.5%	10.0%	2.20%	2.10%	0.00%

$\tau_b = 0.8$ and EI_{eff} is the flexural rigidity used within the column curve for determination of axial compression strength. Further reductions to the stiffness would help eliminate the observed unconservative errors. An example alternative stiffness reduction factor, τ_b, is shown in Equation 3:

$$\tau_b = 1.25 - \frac{M_r}{M_n}\left(1 - 3\frac{P_r}{P_{no}}\right) \leq 0.8 \quad (3)$$

This equation is based on prior work (Denavit and Hajjar, 2014). Data on the secant flexural rigidity was computed based on results from second-order inelastic analysis; an equation was then fit to the data. The variation of the τ_b described by Equation 3 with internal forces is shown in Figure 7. The reduction factor is a constant $\tau_b = 0.8$ for much of the range. Only with high bending moment and low axial loads, where high levels of cracking are expected, does τ_b become less than 0.8 and vary with the axial compression and bending moment.

Performing an elastic analysis with a stiffness reduction that varies with internal forces can be cumbersome. However, there is precedent in U.S. practice. For structural steel members, the factor τ_b varies with axial compression. For reinforced concrete members, the ACI *Building Code Requirements for Structural Concrete and Commentary* (ACI, 2019) includes provisions for an effective flexural rigidity that varies with both axial compression and bending moment.

The effect of the alternative stiffness reduction on the maximum permitted applied loads for the example SRC cross section is shown in Figure 8(a). The solid lines represent the maximum permitted applied loads using a constant $\tau_b = 0.8$; the dashed lines represent the maximum permitted applied loads using Equation 3. The percentage difference between the two is shown in Figure 8(b). The reduction is sufficient to eliminate the unconservative error [e.g., as shown in Figure 6(b).] There are also other attractive features. The alternative stiffness reduction has no effect on the pure bending strength, nor does it affect the strength when the axial compression is high. Also, as seen in Figure 8(b), it has a greater effect on more slender members, for which additional conservatism is likely warranted. The specific factors in Equation 3 should be refined and a wide ranging evaluation should be performed to ensure safety and accuracy, but these limited results show the promise of a moment-based stiffness reduction in efficiently eliminating some of the largest unconservative errors observed in the design provisions for steel-concrete composite framing systems.

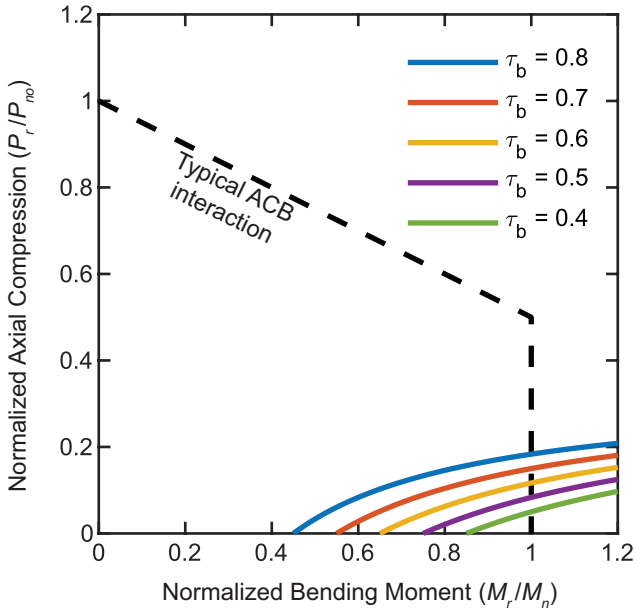

Fig. 7. Contour plot showing the variation of the alternative stiffness reduction factor.

CONCLUSIONS

This work has highlighted some of the most pressing unresolved issues in stability and strength design of steel-concrete composite framing systems: (1) the large conservative errors that result from neglecting the balance point in the calculation of available strength and (2) the large unconservative errors that result from overestimation of the stiffness for very slender concrete-dominant members subjected to high bending moments. An alternative method of computing the available strength interaction diagram was proposed and evaluated against second-order inelastic analyses for a broad range of cases. The results show that using the proposed interaction diagram reduces the largest conservative errors but worsens existing unconservative errors. To address this issue, an alternative stiffness reduction that varies with internal forces was proposed to better capture the occurrence of high levels of cracking and eliminate the unconservative errors. Initial studies with this alternative stiffness reduction showed promising results. Both alternative approaches, once fully validated, have the potential to improve the accuracy and safety of the stability design provisions for steel-concrete composite framing. They can also set the stage for future developments such as design provisions based on cross-section strength and the use of high-strength materials.

REFERENCES

ACI (2019), *Building Code Requirements for Structural Concrete and Commentary*, American Concrete Institute, Farmington Hills, Mich.

AISC (1986), *Load and Resistance Factor Design Specification for Structural Steel Buildings*, American Institute of Steel Construction, Chicago, Ill.

AISC (2005), *Specification for Structural Steel Buildings*, ANSI/AISC 360-05, American Institute of Steel Construction, Chicago, Ill.

AISC (2016), *Specification for Structural Steel Buildings*, ANSI/AISC 360-16, American Institute of Steel Construction, Chicago, Ill.

AISC (2017), *Steel Construction Manual,* 15th Ed., American Institute of Steel Construction, Chicago, Ill.

ASCE (1997), *Effective Length and Notional Load Approaches for Assessing Frame Stability: Implications for American Steel Design*, American Society of Civil Engineers, Reston, Va.

Behnam, A. and Denavit, M.D. (2020), "Plastic Stress Distribution Method for Predicting Interaction Strength of Steel-Concrete Composite Cross Sections," *Journal of Constructional Steel Research*, Vol. 170, 106092.

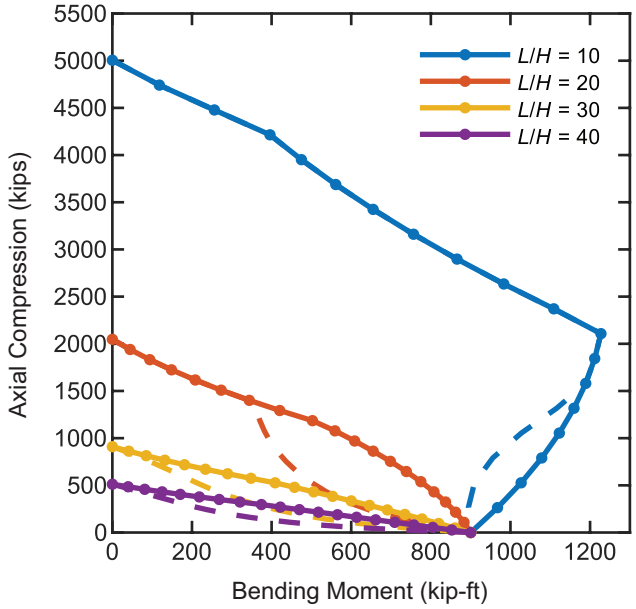

(a) Maximum permitted applied loads with and without the alternative stiffness reduction

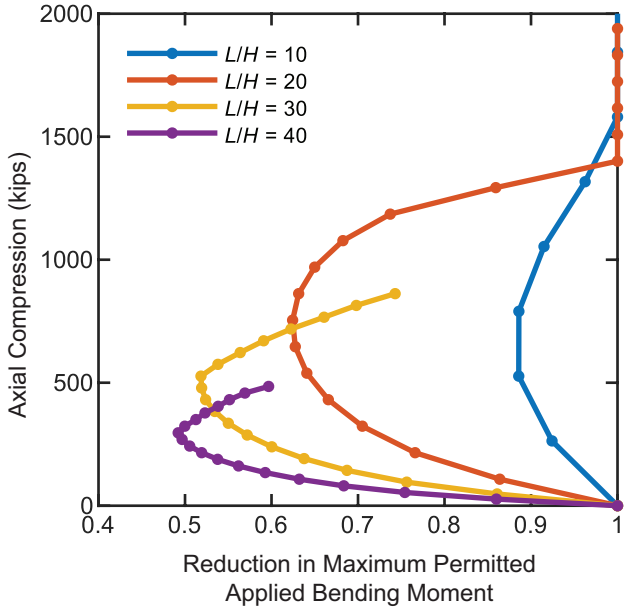

(b) Reduction in maximum permitted applied loads from use of the alternative stiffness reduction

Fig. 8. Results using the alternative stiffness reduction.

Bruneau, M., Kenarangi, H., and Murphy, T.P. (2018), *Contribution of Steel Casing to Single Shaft Foundation Structural Resistance*, NCHRP Research Report 872, The National Academies Press.

CEN (2004), *Eurocode 4: Design of Composite Steel and Concrete Structures—Part 1-1: General Rules and Rules for Buildings*, EN1994-1-1, European Committee for Standardization, Brussels, Belgium.

Denavit, M.D. (2017), "Structural Reliability of Steel-Concrete Composite Columns and Frames," *Proceedings of the 8th International Conference on Composite Construction in Steel and Concrete*, Jackson, Wyo.

Denavit, M.D. and Hajjar, J.F. (2014), *Characterization of Behavior of Steel-Concrete Composite Members and Frames with Applications for Design*, Newmark Structural Laboratory Report Series, Newmark Structural Laboratory Report NSEL-034, University of Illinois at Urbana-Champaign, Urbana, Ill.

Denavit, M.D., Hajjar, J.F., Perea, T., and Leon, R.T. (2016), "Stability Analysis and Design of Composite Structures," *Journal of Structural Engineering*, ASCE, Vol. 142, No. 3, 04015157.

Griffis, L.G. (1992), "Composite Frame Construction," *Constructional Steel Design: An International Guide*, Elsevier Applied Science, London, UK, pp. 523–553.

Griffis, L.G. (2005), "Composite Design Provisions 2005 AISC Specification for Steel Buildings," *Proceedings of the 2005 Structures Congress*, ASCE, New York, N.Y.

Hage, S.E. and MacGregor, J.G. (1974), *The Second-Order Analysis of Reinforced Concrete Frames*, Structural Engineering Report No. 49, Department of Civil Engineering, University of Alberta, Edmonton, Alberta, Canada.

Kanchanalai, T. (1977), *The Design and Behavior of Beam-Columns in Unbraced Steel Frames*, CESRL Report No. 77-2, Structures Research Laboratory, Department of Civil Engineering, The University of Texas at Austin, Austin, Tex.

Lai, Z., and Varma, A.H. (2016). "Effective Stress-Strain Relationships for Analysis of Noncompact and Slender Filled Composite (CFT) Members," *Engineering Structures*, Vol. 124, pp. 457–472.

Lai, Z., Varma, A., and Griffis, L. (2015), "Analysis and Design of Noncompact and Slender CFT Beam-Columns," *Journal of Structural Engineering*, ASCE, Vol. 142, No. 1, 04015097.

SAC (2014), *Technical Code for Concrete Filled Steel Tubular Structures*, GB 50936-2014, Standardization Administration of the People's Republic of China, Beijing, China.

Surovek-Maleck, A.E. and White, D.W. (2004), "Alternative Approaches for Elastic Analysis and Design of Steel Frames. II: Verification Studies," *Journal of Structural Engineering*, ASCE, Vol. 130, No. 8, pp. 1,197–1,205.

Traut-Todaro, J. (2019), "SpeedCore: Lateral System Innovation for Today's Construction Challenges," *Structure Magazine*, November, pp. 12–14.

Wang, Y. and Ziemian, R.D. (2019), "Design by Advanced Elastic Analysis—An Investigation of Beam-Columns Resisting Minor-Axis Bending," *Proceedings of the Annual Stability Conference*, Structural Stability Research Council, St. Louis, Mo.